

Supplementary Material for:

**Solvent modified spin crossover in an iron(III) complex:
phase changes and an exceptionally wide hysteresis**

Wasinee Phonsri,^a Phimphaka Harding,^a Lujia Liu,^b Shane G. Telfer,^b
Keith S. Murray,^c Boujema Moubarak,^c Tamsyn M. Ross,^d
Guy N. L. Jameson^e and David J. Harding*^a

E-mail: hdavid@g-mail.wu.ac.th

^a *Functional Materials and Nanotechnology Centre of Excellence (FuNTech), Walailak University, Thasala, Nakhon Si Thammarat, 80160, Thailand.*

^b *MacDiarmid Institute for Advanced Materials and Nanotechnology, Institute of Fundamental Sciences, Massey University, Palmerston North, New Zealand.*

^c *School of Chemistry, Monash University, Clayton, Melbourne, Victoria, 3800, Australia.*

^d *Australian Synchrotron, 800 Blackburn Rd, Clayton, Victoria, 3168, Australia.*

^e *Department of Chemistry & MacDiarmid Institute for Advanced Materials and Nanotechnology, University of Otago, PO Box 56, Dunedin, 9054, New Zealand.*

Table S1 Crystallographic data and structure refinement for [Fe(qsal-I)₂]OTf·solvent.

Solvent	MeOH, 1		EtOH, 2b		EtOH, 2a	
	163 K/LS	293 K/HS	100 K/LS	170 K/HS1	213 K/HS2	292 K/HS3
Formula	C ₃₄ H ₂₄ F ₃ FeI ₂ N ₄ O ₆ S	C ₃₄ H ₂₄ F ₃ FeI ₂ N ₄ O ₆ S	C ₃₅ H ₂₆ F ₃ FeI ₂ N ₄ O ₆ S	C ₃₅ H ₂₆ F ₃ FeI ₂ N ₄ O ₆ S	C ₃₅ H ₂₆ F ₃ FeI ₂ N ₄ O ₆ S	C ₃₅ H ₂₆ F ₃ FeI ₂ N ₄ O ₆ S
Molecular weight / g mol ⁻¹	982.79	982.79	997.31	997.31	997.31	997.31
Crystal system	Triclinic	Triclinic	Triclinic	Triclinic	Triclinic	Triclinic
Space group	P ⁻ 1					
<i>a</i> / Å	12.2488(5)	11.7726(4)	12.430(3)	11.4760(12)	11.5003(2)	11.5289(9)
<i>b</i> / Å	12.3956(4)	12.6918(4)	12.336(3)	13.0698(16)	13.1342(3)	13.1814(11)
<i>c</i> / Å	12.8192(9)	13.3179(9)	13.183(3)	13.4649(16)	13.5498(10)	13.6233(12)
α / °	70.108(5)	69.437(5)	111.83(3)	71.342(11)	71.652(5)	71.947(5)
β / °	87.581(6)	85.020(6)	99.23(3)	87.437(9)	87.488(6)	87.644(6)
γ / °	68.745(5)	67.526(5)	66.05(3)	68.674(11)	68.858(5)	68.871(5)
Cell volume / Å ³	1698.40(15)	1719.03(14)	1714.8(6)	1776.5(4)	1806.23(14)	1830.2(3)
<i>Z</i>	2	2	2	2	2	2
Absorption coefficient / mm ⁻¹	19.012	18.784	2.371	2.289	17.887	17.653
Reflections collected	19123	21734	34873	14824	25586	20681
Independent reflections, <i>R</i> _{int}	6290, 0.0875	4843, 0.0681	9063, 0.1036	8087, 0.0348	6749, 0.0986	5882, 0.1696
Max. and min. transmission	1.0 and 0.57	1.0 and 0.34		0.7708 and 0.5985	0.2045 and 0.0944	
Restraints/parameters	6/462	12/462	0/471	0/470	54/472	0/470
Final R indices [$>2\sigma(I)$]: <i>R</i> ₁ , <i>wR</i> ₂	0.0969, 0.3147	0.0715, 0.2346	0.0578, 0.1616	0.0433, 0.1101	0.0846, 0.2623	0.0816, 0.2323

Table S1 Crystallographic data and structure refinement for [Fe(qsal-I)₂]OTf·solvent (continued).

Solvent	<i>n</i> -PrOH, 3		<i>i</i> -PrOH, 4		Acetone, 5		MeCN, 6
	100 K/LS	270 K/HS	163 K/LS	293 K/mostly HS	137 K/LS	293 K/mostly HS	123 K/LS
Formula	C ₃₆ H ₂₈ F ₃ FeI ₂ N ₄ O ₆ S	C ₃₆ H ₂₈ F ₃ FeI ₂ N ₄ O ₆ S	C ₃₆ H ₂₈ F ₃ FeI ₂ N ₄ O ₆ S	C ₃₆ H ₂₈ F ₃ FeI ₂ N ₄ O ₆ S	C ₃₆ H ₂₆ F ₃ FeI ₂ N ₄ O ₆ S	C ₃₆ H ₂₆ F ₃ FeI ₂ N ₄ O ₆ S	C ₃₅ H ₂₃ F ₃ FeI ₂ N ₅ O ₅ S
Molecular weight /	1011.33	1011.33	1011.33	1011.33	1009.32	1009.32	992.29
Crystal system	Triclinic						
Space group	P $\bar{1}$						
<i>a</i> / Å	12.232(2)	12.4864(12)	12.2308(2)	12.4632(3)	10.3759(4)	10.3585(6)	12.0127(13)
<i>b</i> / Å	12.547(3)	12.4925(12)	12.6838(2)	12.6561(3)	12.8053(5)	12.9759(6)	12.6193(13)
<i>c</i> / Å	13.279(3)	13.6444(12)	13.0436(9)	13.3650(9)	13.8091(10)	14.1074(3)	13.2123(14)
α / °	81.89(3)	65.751(9)	83.137(6)	83.298(6)	79.080(6)	78.558(6)	110.546(4)
β / °	67.04(3)	82.594(7)	68.061(5)	67.300(5)	76.267(5)	76.606(6)	92.310(4)
γ / °	68.25(3)	69.191(9)	70.096(5)	69.644(5)	86.609(6)	86.265(4)	111.271(2)
Cell volume / Å ³	1742.9(6)	1813.6(3)	1764.77(13)	1823.00(14)	1749.85(16)	1807.59(14)	1715.2(3)
Z	2	2	2	2	2	2	2
Absorption coefficient / mm ⁻¹	2.334	2.243	18.318	17.733	18.474	17.8884	2.369
Reflections collected	73090	16431	24041	25636	24183	24662	11294
Independent reflections, <i>R</i> _{int}	11762, 0.0383	8529, 0.0259	6611, 0.0693	6809, 0.0860	6466, 0.094	6066, 0.095	7642, 0.0223
Max. and min. transmission	0.9548 and 0.9333	1.0000 and 0.8949	1.000 and 0.303	1.000 and 0.486	1.0000 and 0.1871	1.0000 and 0.1349	0.753 and 0.497
Restraints/parameters	0/471	0/479	58/499	72/499	121/480	129/480	0/470
Final R indices	0.0500, 0.1305	0.0480, 0.1397	0.0801, 0.2665	0.0805, 0.2622	0.0822, 0.2481	0.0819, 0.2643	0.0539, 0.1470

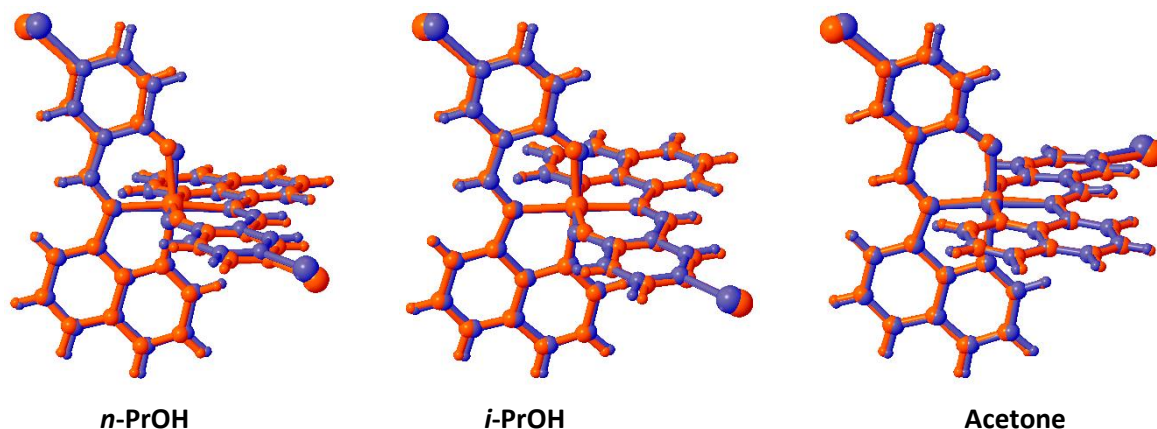


Figure S1 Overlay of the HS and LS structures for **3** (left), **4** (middle) and **5** (right).

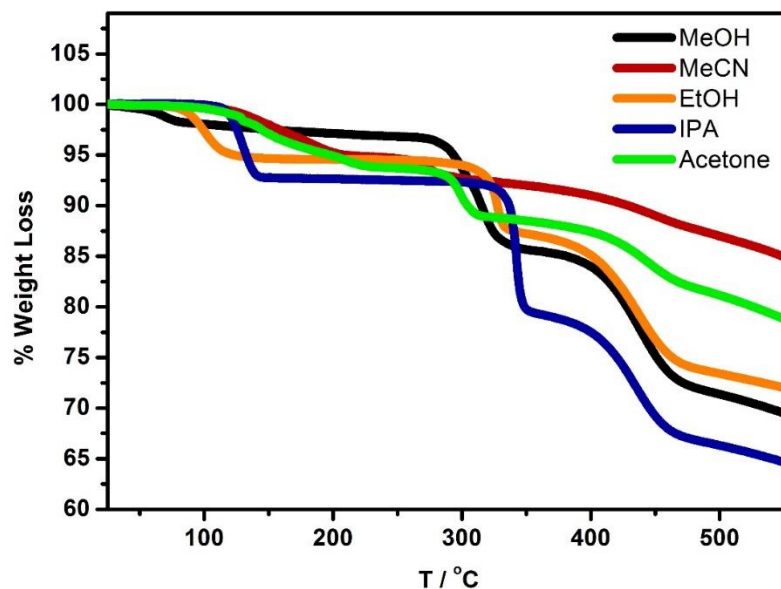
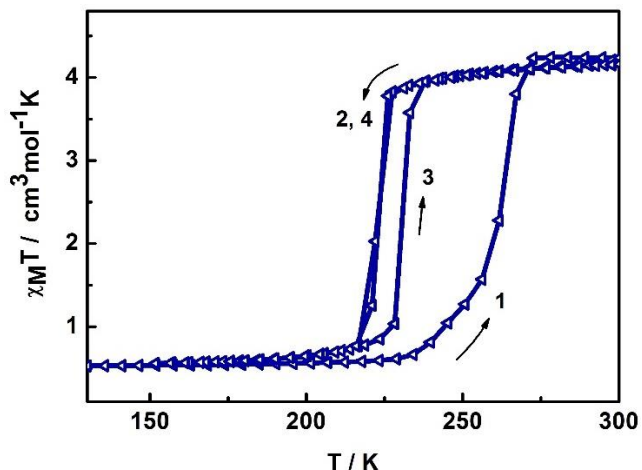


Figure S2 TGA analysis of $[\text{Fe}(\text{qsal-I})_2]\text{OTf}\cdot\text{sol}$ (sol = MeOH, EtOH, *i*-PrOH, MeCN, Acetone).

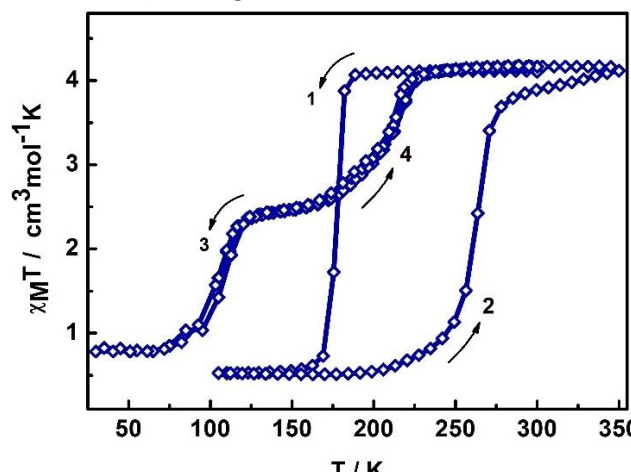
TGA studies on these compounds reveal that the solvent significantly affects the thermal stability of the system. The EtOH solvate shows solvent loss occurring at 353 K. In contrast, the *i*-PrOH solvate doesn't lose any solvent until 402 K suggesting that the higher boiling *i*-PrOH imparts greater thermal stability. The MeCN and acetone solvates show more gradual solvent loss which is centred at 434 and 402 K, respectively. It follows that the solvent's shape, boiling point and ability to hydrogen bond all play a role in the thermal stability of $[\text{Fe}(\text{qsal-I})_2]\text{OTf}\cdot\text{sol}$.

SQUID and DSC measurements



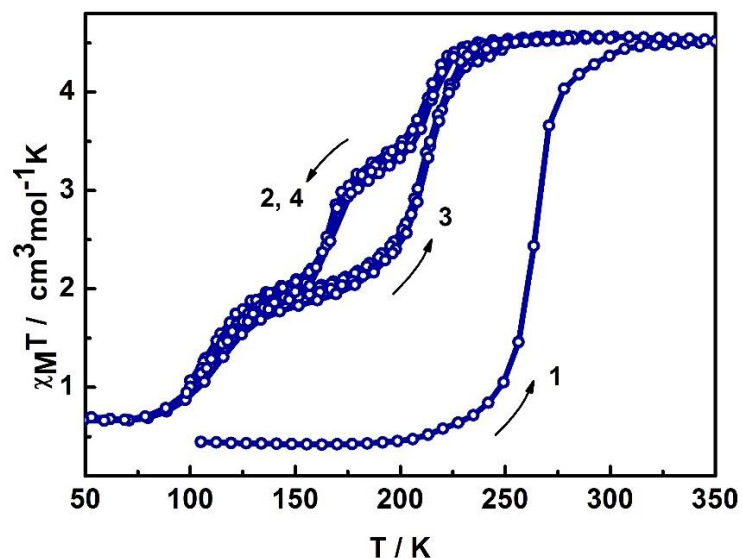
a) Desolvated **2** (Heating at 100 C for 1.5 hrs under vacuum).

cycle	$T_{1/2}$ K	
	cool	heat
1 st	222	267
2 nd	221	233



b) Freshly prepared sample, the measurement starting at high temperature.

cycle	$T_{1/2}$ K	
	cool	heat
1 st	175	270
2 nd	213, 103	214, 105
3 rd	213, 103	214, 105



c) Freshly prepared sample, the measurement starting at low temperature.

cycle	$T_{1/2}$ K	
	cool	heat
1 st	-	270
2 nd	208, 175, 107	109, 208
3 rd	208, 175, 108	110, 208
4 th	208, 176, 108	110, 208

Figure S3 The $\chi_M T$ vs T plot and $T_{1/2}$ data for $[Fe(qsal-I)_2]OTf \cdot EtOH$, **2** with different treatments.

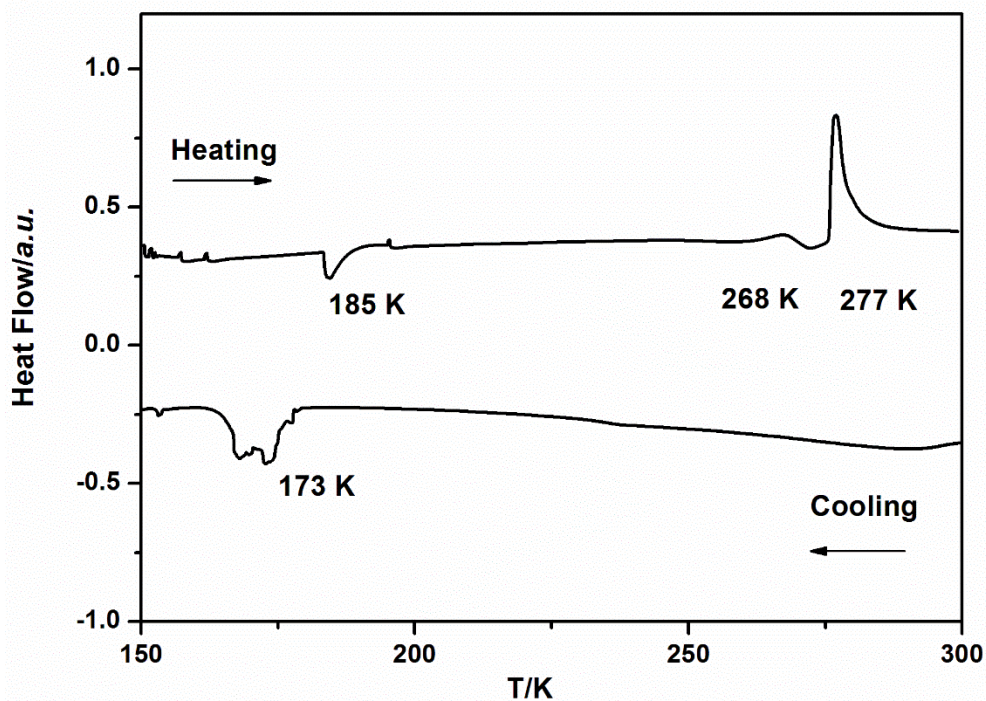


Figure S4 DSC plot for freshly prepared $[\text{Fe}(\text{qsal-}\text{I})_2]\text{OTf}\cdot\text{EtOH}$ run from 303 -113-303 K in cycle 1 (4K/min). The unusual exothermic peak in the heating mode takes place at 185 K. This peak is kinetic appearing at around 203 K at lower scan rates.

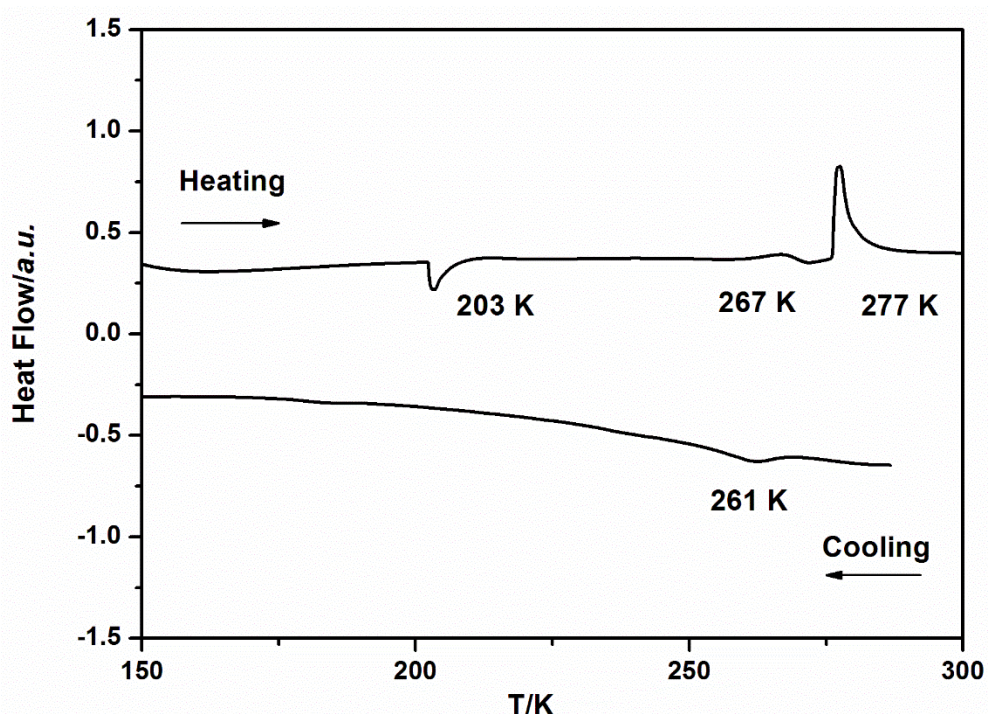


Figure S5 DSC plot for freshly prepared $[\text{Fe}(\text{qsal-}\text{I})_2]\text{OTf}\cdot\text{EtOH}$ run from 303-113-303 K in cycle 2 (similar to cycle 3).

Table S2 Enthalpy and entropy parameters of freshly prepared $[\text{Fe}(\text{qsal-I})_2]\text{OTf}\cdot\text{EtOH}$ in the first cycle.

cycle	$T_{1/2}$ (K)	ΔH (kJ mol ⁻¹)	ΔS (J mol ⁻¹ K ⁻¹)
1	173	7.0	40.5
	277	6.7	24.0
2	277	7.0	24.1

Table S3 Mössbauer spectroscopic data of $[\text{Fe}(\text{qsal-I})_2]\text{OTf}\cdot\text{EtOH}$.

Temperature (K)	Species	δ (mm/s)	ΔE_Q (mm/s)	Γ_L (mm/s)	Γ_R (mm/s)	I (%)
5.3	LS	0.21	2.91	0.28	0.24	100
77	LS	0.21	2.91	0.28	0.24	100
200	LS	0.17	2.88	0.31	0.24	100
293	HS	0.33	0.45	0.49	0.59	100
220	LS	0.16	2.85	0.31	0.25	100
5.3	LS	0.21	2.91	0.28	0.24	100

Variable Temperature Synchrotron Powder Diffraction Studies

General Details

The samples used for variable temperature powder diffraction studies contained impurities. A strongly-diffracting, high-angle impurity was identified in the powder diffraction data, with unit cell and symmetry consistent with KCl; as KCF_3SO_3 was sometimes used instead of AgCF_3SO_3 . Further, a low angle peak (at $2\theta = \sim 2.95$) is present in all diffraction data that does not belong to any of the identified phases on **2**. In order to avoid including these known impurity peaks in refinements, refinements have been performed between $2\theta = 3.5 - 12$. As a result of the impurities in the samples as well as the limited range used for Pawley refinements, no close analysis of the calculated unit cell parameters is included here.

Table S4 Temperatures of data collection and Crystallographic phases present in **Dataset A**.

	Temperature Range	Data Collection Temperatures
Step 1	300 K → 100 K	300 K to 200 K at 10 K intervals; 200 K to 150 K at 2 K intervals; 150 K to 100 K at 10 K intervals Phase 2a present while cooling, until gone at 164 K. Phases 2b and 2c emerge at 180 K.
Step 2	100 K → 300 K	100 K to 200 K at 10 K intervals; 200 K to 300 K at 5 K intervals Phase 2b present across all temperatures. As heated, Phase 2a emerges at 220 K, Phase 2c gone by 215 K.
Step 3	300 K → 95 K	300 K to 230 K at 10 K intervals; 230 K to 95 K at 5 K Phase 2b present across all temperatures. As cooled, Phase 2a gone at 180 K, Phase 2c emerges at 180 K.
Step 4	95 K → 240 K	95 K to 240 K at 5 K intervals Phase 2b present across all temperatures. As heated, Phase 2a emerges at 215 K, Phase 2c gone at 215 K.

Table S5 Temperatures of data collection and Crystallographic phases present in **Dataset B**.

	Temperature Range	Data Collection Temperatures
Step 1	100 K → 300 K	100 K to 200 K at 10 K intervals; 200 K to 300 K at 5 K intervals Phase 2b present across all temperatures. As heated, Phase 2c gone at 215 K, Phase 2a emerges at 210 K.
Step 2	300 K → 80 K	300 K to 230 K at 10 K intervals; 230 K to 85 K at 5 K intervals Phase 2b present across all temperatures. As cooled, Phase 2a gone at 175 K, Phase 2c emerges at 190 K.
Step 3	80 K → 230 K	80 K to 230 K at 5 K intervals Phase 2b present across all temperatures. As heated, Phase 2a emerges at 200 K, Phase 2c gone at 200 K.
Step 4	230 K → 90 K	230 K to 90 K at 5 K intervals Phase 2b present across all temperatures. As cooled, Phase 2a gone at 180 K, Phase 2c emerges at 190 K.

Observation of Phase 2c

Phase **2c** was identified as a result of peaks unassignable to either phase **2a** or phase **2b** emerging in/disappearing from diffraction patterns as temperature was varied. Figures S6 to S7 depict the disappearance of phase **2a** and the appearance of phase **2c** between 200 K and 170 K in step 2 of **Dataset B**. Phase **2c** was primarily identified using the peak at $2\theta = \sim 4.7$, but a peak at $2\theta = \sim 8.5$ is also noted to emerge as the temperature was lowered, thought to also belong to Phase **2c**. Other emergent/disappearing peaks may be observable.

Pawley fitting was performed on representative diffraction patterns from within **Dataset A**. Splitting of the phase **2a** peaks was noted in step 1 diffraction data collected above \sim 166K, and Pawley fitting was performed using a sample displacement correction.¹ Representative Pawley fits are shown in Figures S6, unit cell parameters and R_{wp} and GOF values are given in Table S6.

Table S6 Calculated unit cell parameters, R_{wp} and GOF values from Pawley modelling performed on representative Dataset A diffraction patterns.

Temperature/Step	Phase of Fit	a	b	c	α	β	γ	R_{wp}	GOF
250 K/Step 1	2a	11.4909(6)	13.1742(6)	13.6106(5)	71.730(3)	87.583(4)	68.957(3)	7.456	4.076
180 K/Step 1	2a	11.4571(8)	13.1445 (9)	13.5370(9)	71.603(3)	87.492(2)	68.798(2)	8.271	4.488
100 K/Step1	2b	12.367(2)	12.446(2)	13.210(2)	80.668(4)	68.100(3)	65.703(2)	6.697	3.762

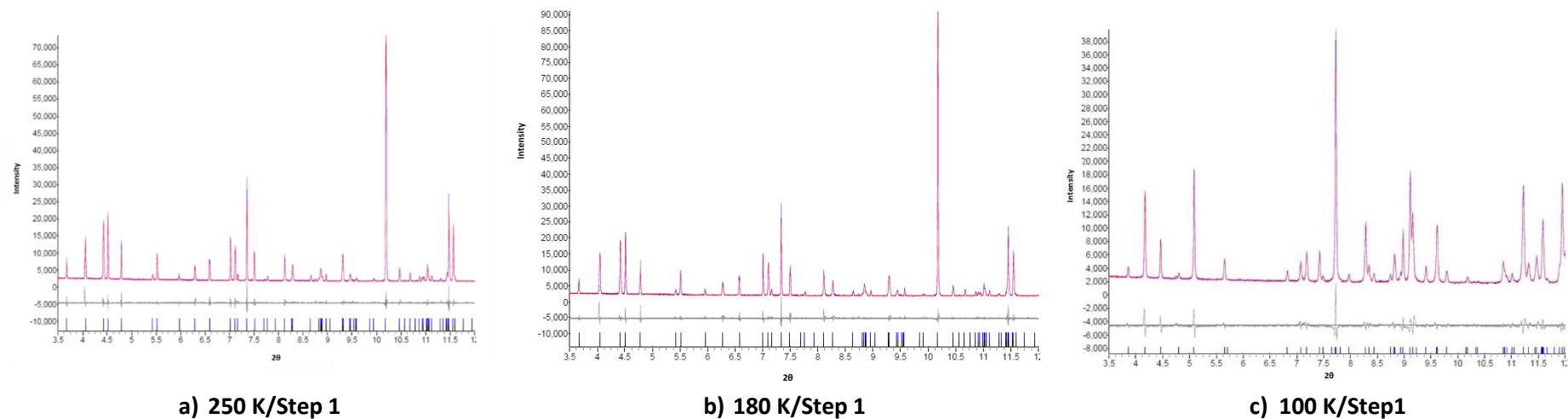


Figure S6 Pawley fit to diffraction pattern collections, as part of step 1 of Dataset A, showing original data (blue line), the fit found for a) and b) **2a** c) **2b** (red line), and the difference between actual and calculated patterns (grey line). Blue/black peak markers showing possible peak locations for a) and b) **2a** c) **2b** are shown at the bottom.

Table S7 Calculated unit cell parameters, R_{wp} and GOF values from Pawley modelling performed on representative Dataset B diffraction patterns.

Temperature/Step	Phase of Fit	a	b	c	α	β	γ	R_{wp}	GOF
150 K/Step1	2b	12.381(1)	12.466(1)	13.216(1)	80.670(1)	68.120(2)	65.847(2)	6.151	4.114
290 K/Step 1	2b	12.544(2)	12.411(2)	13.578(2)	82.498(3)	68.489(3)	65.735(3)	5.971	4.071
290 K/Step 1	2a	11.521(2)	13.191(2)	13.621(2)	71.816(4)	87.616(6)	68.917(4)	-	-
185 K/Step 2	2b	12.397(1)	12.487(1)	13.227(1)	80.774(3)	68.209(4)	66.076(4)	5.629	3.831
185 K/Step 2	2a	11.484(2)	13.130(1)	13.520(1)	71.568(5)	87.457(7)	68.755(6)	-	-
100 K/Step 3	2b	12.368(2)	12.448(2)	13.205(2)	80.721(4)	68.136(3)	65.723(2)	8.182	5.475
230 K/Step 3	2b	12.428(1)	12.512(1)	13.247(1)	81.009(2)	68.374(2)	66.336(2)	4.256	2.894
230 K/Step 3	2a	11.518(2)	13.111(2)	13.596(2)	71.55(1)	87.19(2)	69.03(1)	-	-

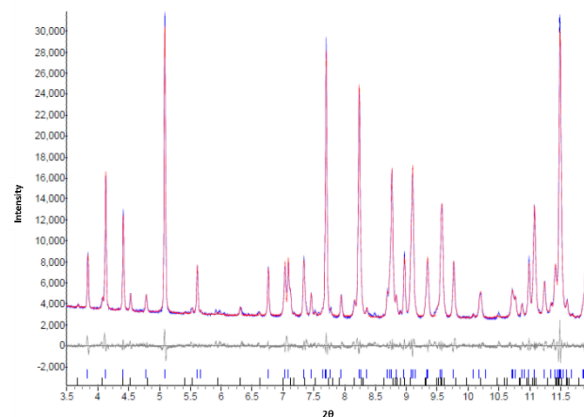
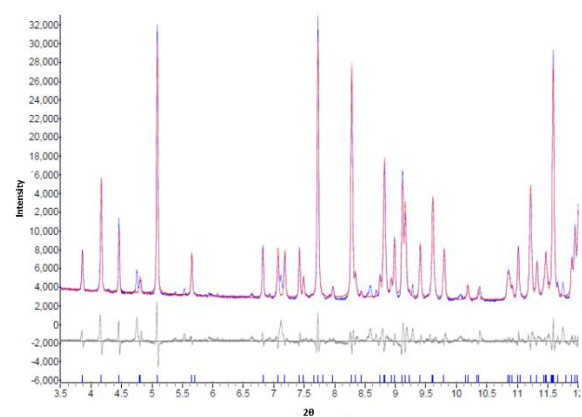
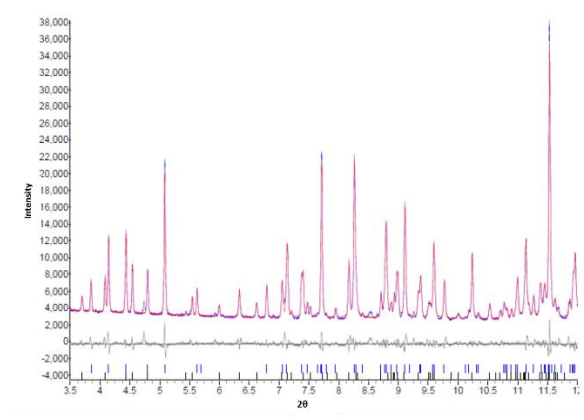
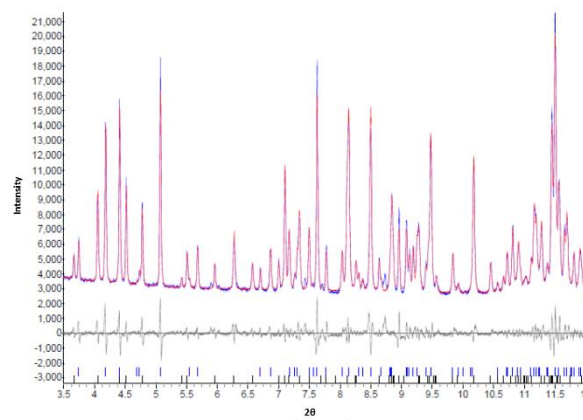
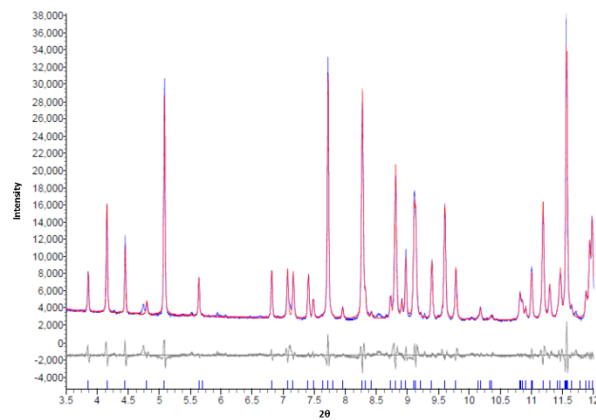


Figure S7 Pawley fit to diffraction pattern collectetions at various temperatures, of Dataset B, showing original data (blue line), the fit found for a) and d) are **2b** (red line) and the difference between actual and calculated patterns (grey line). Blue peak markers showing possible peak locations for **2b** are shown at the bottom. The fit found for b), c) and e) are **2a/2b** (red line) and the difference between actual and calculated patterns (grey line). Blue peak markers showing possible peak locations for **2b** are shown at the bottom, and black peak markers showing possible peak locations for **2a** are shown at the bottom.

References

1. N. V. Y. Scarlett, M. R. Rowles, K. S. Wallwork and I. C. Madsen, *J. Appl. Cryst.*, 2011, **44**, 60-64.

Table S8 Intermolecular interactions within **1** at 163, 230 and 293 K.

Interactions	163 K	230 K	293 K
Connect into chain along b axis			
$\pi\cdots\pi$	3.270	3.320	3.399
$ I_1\cdots\pi$	3.665	3.680	3.769
O20…H7	2.693(10)	2.748(6)	2.865(8)
O20…C7	3.390(17)	3.447(12)	3.722(14)
$\angle O20\cdots H7-C7$	148.6(8)	147.5(5)	153.7(6)
$\pi\cdots\pi$	3.280	3.266	3.354
O1…H26	2.506(10)	2.535(8)	2.729(8)
O1…C26	3.381(18)	3.386(13)	3.556(15)
$\angle O1\cdots H26-C26$	153.1(8)	150.8(6)	148.7(7)
Connect into chain along a axis			
P4AE			
$\pi\cdots\pi$	3.371	3.366	3.468
C33-H33… π	2.467	2.513	2.569
Connect into chain along c axis			
CF₃SO₃ interactions			
O100…H22	2.520(10)	2.529(9)	2.818(12)
O100…C22	3.264(15)	3.260(12)	3.472(16)
$\angle O100\cdots H22-C22$	135.2(9)	134.7(7)	128.3(9)
O100…H11	2.545(12)	2.581(1)	2.474(14)
O100…C11	3.180(22)	3.216(15)	3.172(20)
$\angle O100\cdots H11-C11$	124.4(10)	125.2(6)	131.9(9)
O101…H34	2.489(14)	2.550(11)	2.589(18)
O101…C34	3.297(22)	3.343(17)	3.393(24)

Interactions	163 K	230 K	293 K
$\angle O101\cdots H34-C34$	142.8(8)	142.2(6)	145.1(9)
O102…H21	2.639(9)	2.639(8)	2.698(11)
O102…C21	3.430(16)	3.436(12)	3.608(16)
$\angle O102\cdots H21-C21$	141.1(8)	143.0(6)	165.8(7)
O102…C7	3.123(16)	3.117(11)	3.019(15)
O102…H35	2.504(11)	2.520(10)	2.613(14)
O102…C35	3.394(19)	3.406(16)	3.487(21)
$\angle O102\cdots H35-C35$	156.1(8)	157.2(7)	156.8(8)
F2…H15	2.485(9)	2.488(7)	2.629(13)
F2…C15	3.356(16)	3.362(12)	3.538(18)
$\angle F2\cdots H15-C15$	152.4(8)	154.4(6)	165.7(7)
MeOH interactions			
O200…H2	2.612(13)	2.634(11)	2.700(17)
O200…C2	3.407(21)	3.432(16)	3.580(23)
$\angle O200\cdots H2-C2$	141.5(9)	143.1(6)	158.1(8)
O200…H16	2.412(14)	2.438(12)	2.586(18)
O200…C16	3.292(20)	3.308(16)	3.450(24)
$\angle O200\cdots H16-C16$	153.9(8)	153.6(6)	154.6(9)
O200…C28	3.175(13)	3.258(12)	3.401(15)
MeOH-CF₃SO₃			
O101…H200	2.087(9)	2.014(6)	2.089(10)
O101…O200	2.765(13)	2.781(10)	2.742(15)
$\angle O101\cdots H200-O200$	137.5(8)	153.5(7)	136.3(11)

Table S9 Intermolecular interactions within **2** at 100, 170, 213 and 292 K.

	100 K	170 K	213 K	292 K
1D chain along the <i>b</i> axis				
$\pi\cdots\pi$	3.310	3.384	3.403	3.431
O1…H25	2.579(3)	2.402(4)	2.427(9)	2.444(8)
O1…C25	3.462(6)	3.274(7)	3.262(15)	3.267(14)
\angle O1…H25-C25	154.9(4)	152.2(3)	149.4(7)	147.4(7)
O1…H23	2.503(4)			
O1…C23	3.359(6)			
\angle O1…H23-C23	150.0(3)			
I1… π	3.772(6)	3.607(4)	3.645(8)	3.668(8)
$\pi\cdots\pi$	3.243	3.365	3.405	3.444
O2…H7	2.623(5)			
O2…C7	3.483(8)			
\angle O2…H7-C7	150.8(3)			
2D chain along the <i>a</i> axis				
P4AE				
C29-H29… π (C8-C12)	2.607	2.540	2.592	2.625
$\pi\cdots\pi$	3.062	3.444	3.467	3.514
O5… π	3.022(5)	-	-	-
2D chain along <i>c</i> axis				
I1…I1	-	3.7086(8)	3.6796(13)	3.6698(14)
OTf and EtOH in 1D				
I2…O4	-	3.282(4)	3.288(10)	3.276(9)
I1…H33A	-	3.0990(7)	3.1509(6)	3.2349(7)

I1…C33	-	4.068(5)	4.096(12)	4.172(12)
\angle I1…H33A-C33	-	166.4(4)	165.3(9)	163.2(9)
F2…F2	2.719(8)	2.865(5)	2.905(13)	2.925(10)
O3…H7	2.785(5)	2.604(3)	2.625(8)	2.682(7)
O3…C7	3.055(7)	2.921(6)	2.956(13)	2.995(12)
\angle O3…H7-C7	97.3(4)	99.9(3)	101.1(6)	100.7(6)
O3…H18	2.539(6)			
O3…C18	3.308(10)			
\angle O3…H18-C18	138.2(4)			
O3…H31	2.500(6)			
O3…C31	3.415(10)			
\angle O3…H31-C31	161.8(4)			
Interactions				
O4…H19	2.598(7)			
O4…C19	3.311(11)			
\angle O4…H19-C19	132.2(4)			
O5…H30	2.361(6)			
O5…C30	3.130(9)			
\angle O5…H30-C30	137.7(4)			
O4…H11	-	2.377(5)	2.418(12)	2.412(11)
O4…C11	-	3.142(8)	3.159(17)	3.169(14)
\angle O4…H11-C11	-	137.2(4)	136.6(8)	138.4(7)
O5…H6	-	2.052(4)	2.103(8)	2.086(7)
O5…O6	-	2.781(5)	2.817(11)	2.794(9)
\angle O5…H6-O6	-	144.8(3)	145.5(8)	144.7(7)
O4…H6	2.109(6)			

O4···O6	2.913(8)
∠ O4···H6-O6	160.3(5)
O6···H15	2.530(8)
O6···C15	3.427(10)
∠ O6···H15-C15	157.7(4)
O6···H23	-
O6···C23	-
∠ O6···H23-C23	-
O6···C25	3.017(8)
	3.179(5)
	3.190(12)
	3.246(13)

Table S10 Intermolecular interactions within **3** at 100 and 270 K.

Interactions	100K	270 K
Connect into chain along <i>a</i> axis		
$\pi\text{-}\pi$	3.184	3.268
H5....O2	2.661(2)	2.659(4)
C5....O2	3.450(5)	3.458(6)
\angle C5-H5....O2	140.8(2)	144.6(3)
H7....O2	2.590(2)	3.039(4)
C7....O2	3.409(4)	3.781(6)
\angle C7-H7....O2	144.5(3)	137.9(3)
$\pi\text{-}\pi$	3.232	3.331
H23....O1	2.642(3)	2.782(5)
C23....O1	3.483(6)	3.601(7)
\angle C23-H23....O1	147.9(3)	147.7(3)
1D chain along <i>b</i> axis		
P4AE		
$\pi\text{-}\pi$	3.091	3.255
C13-H13.... π	2.578	2.598
Connect into chain along <i>c</i> axis via CF₃SO₃		
C23O3	3.048(4)	2.980(5)
H2....O3	2.625(4)	2.702(5)
C2....O3	3.389(6)	3.527(8)
\angle C2-H2....O3	137.8(2)	148.1(3)
H15....O3	2.500(4)	2.741(6)
C15....O3	3.417(6)	3.639(9)
\angle C15-H15....O3	162.4(3)	163.0(4)
H14....O4	2.399(4)	2.593(6)
C14....O4	3.174(6)	3.340(9)
\angle C14-H14....O4	138.6(3)	137.6(4)
H3....O5	2.689(5)	3.061(7)
C3....O5	3.372(6)	3.677(9)

Interactions	100K	270 K
\angle C3-H3....O5	129.3(2)	125.2(4)
H2....F3	2.629(3)	2.813(5)
C2....F3	3.248(5)	3.460(8)
\angle C2-H2....F3	123.2(2)	127.6(3)
C9....O6	2.938(4)	3.053(8)
C12....O4	3.162(4)	
C16....O4	3.048(4)	
C31....O4	3.006(5)	
F2....F2	2.713(4)	2.8091(58)
n-PrOH		
H31....O6	2.618(3)	3.017(10)
C31....O6	3.522(5)	3.918(11)
\angle C31-H31....O6	159.2(3)	163.2(4)
H36B....I1	2.972(1)	3.112(5)
C36I1	3.724(3)	3.868(10)
\angle C36-H36B....I1	134.4(1)	136.9(6)
C34....I1	3.666(3)	3.821(10)
n-PrOH-CF₃SO₃		
H6....O5	2.162(3)	2.200(5)
O6....O5	2.980(4)	2.981(8)
\angle O6-H6....O5	163.0(2)	159.3(5)
H34A....F1	2.540(3)	2.724(4)
C34....F1	3.483(3)	3.5987(8)
\angle C34-H34A....F1	159.1(1)	150.0(5)
H36C....O5	2.653(4)	2.922(6)
C36....O5	3.224(5)	3.459(12)
\angle C36-H36C....O5	117.4(2)	116.5(5)

Table S11 Intermolecular interactions within **4** at 163 and 293 K.

Interactions	163 K	293 K	Interactions	163 K	293 K
1D chain along α axis					
$\pi\cdots\pi$	3.230	3.317	I1 \cdots H20C	2.675(33)	2.700(35)
O2 \cdots H15	2.648(7)	2.801(6)	I1 \cdots C201	3.747(11)	3.782(12)
O2 \cdots C15	3.443(14)	3.597(12)	\angle I1 \cdots H20C-C201	165.4(19)	168.0(19)
\angle O2 \cdots H15-C15	141.6(8)	142.0(7)	I2 \cdots H20F	3.367(4)	3.154(28)
O2 \cdots H17	2.622(8)	2.775(6)	I2 \cdots C202	4.127(11)	4.124(11)
O2 \cdots C17	3.430(15)	3.583(12)	\angle I2 \cdots H20F-C202	127.3(12)	147.8(14)
\angle O2 \cdots H17-C17	143.3(9)	143.5(7)	C32 \cdots H20D	3.222(26)	2.863(19)
C32 \cdots H15	2.826(16)	2.925(13)	C32 \cdots C202	3.844(12)	3.805(12)
C32 \cdots C15	3.721(21)	3.842(18)	\angle C32 \cdots H20D-C202	116.8(17)	144.3(9)
\angle C32 \cdots H15-C15	157.4(8)	162.8(7)	O102 \cdots H37	2.778(7)	2.667(6)
$\pi\cdots\pi$	3.228	3.285	O102 \cdots C37	3.037(11)	2.982(5)
O1 \cdots H37	2.692(10)	2.838(9)	\angle O102 \cdots H37-C37	96.6(6)	99.9(5)
O1 \cdots C37	3.517(16)	3.666(14)	I2 \cdots I2	4.009(11)	3.890(2)
\angle O1 \cdots H37-C37	145.5(7)	146.0(7)	<i>i</i>-PrOH-CF_3SO_3 interactions		
1D chain along b axis			O101 \cdots H200	2.020(8)	1.903(8)
C26-H26 \cdots π	2.762	2.783	O101 \cdots O200	2.812(13)	2.705(14)
<i>i</i>-PrOH-CF_3SO_3			\angle O101 \cdots H200-O200	156.8(7)	159.4(8)
O102 \cdots H28	2.460(11)	2.594(10)	F101 \cdots H20G	2.826(12)	2.641(12)
O102 \cdots C28	3.375(18)	3.513(17)	F101 \cdots C200	3.697(9)	3.620(10)
\angle O102 \cdots H28-C28	161.6(9)	162.8(8)	\angle F101 \cdots H20G-C200	136.0(9)	147.7(92)
O100 \cdots H27	2.481(10)	2.656(13)	F100 \cdots H20E	2.571(18)	3.440(18)
O100 \cdots C27	3.270(17)	3.422(20)	F100 \cdots C202	3.549(11)	3.726(12)
\angle O100 \cdots H27-C27	140.6(8)	137.9(9)	\angle F100 \cdots H20E-C202	148.1(15)	96.5(11)
O100 \cdots C29	3.129(11)	3.152(10)	F101 \cdots F101	2.760(11)	2.843(10)
O100 \cdots C48	3.090(13)	3.150(13)			
O100 \cdots C25	3.197(11)	3.265(11)			

Table S12 Intermolecular interactions within **5** at 137 and 293 K.

Interactions	137 K	293 K	Interactions	137 K	293 K
Chain along b axis					
$\pi \cdots \pi$	3.263	3.395	O01···H46	2.480(13)	2.552(12)
O1···H42	2.537(8)	2.556(8)	O01···C46	3.409(16)	3.464(17)
O1···C42	3.405(13)	3.412(14)	\angle O01···H46-C46	165.8(6)	161.4(8)
\angle O1···H42-C42	152.0(6)	153.4(6)	F03···I2	3.302(20)	3.545(17)
$\pi \cdots \pi$	3.163	3.313	O02···I2	3.365(22)	3.521(18)
O2···H17	2.499(6)	2.571(8)	CF₃SO₃-CF₃SO₃		
O2···C17	3.382(12)	3.422(12)	O03···F02	2.559(28)	2.525(24)
\angle O2···H17-C17	154.9(6)	152.4(6)	O03···C01	2.793(37)	3.126(34)
Chain along a axis			\angle O03···F02-C01	84.9(15)	105.7(14)
P4AE			O03···F03	2.648(31)	3.250(28)
$\pi \cdots \pi$	3.551	3.606	O03···C01	2.793(37)	3.126(34)
C44-H44··· π	3.179	3.303	\angle O03···F03-C01	81.6(18)	73.1(16)
Chain along c axis			O03···S01	2.882(20)	3.366(18)
I1···I1	3.861(1)	3.916(1)	Acetone		
CF₃SO₃			O04···H48	2.632(10)	2.779(12)
O03···H13	2.716(20)	2.969(17)	O04···C48	3.321(15)	3.494(17)
O03···C13	3.532(22)	3.684(20)	\angle O04···H48-C48	129.7(7)	134.4(7)
\angle O03···H13-C13	144.4(8)	134.8(8)	O04···H24	2.466(8)	2.515(9)
O01···H28	2.394(14)	2.635(12)	O04···C24	3.356(13)	3.374(14)
O01···C28	3.290(18)	3.525(17)	\angle O04···H24-C24	156.1(7)	153.8(8)
\angle O01···H28-C28	157.0(7)	160.6(7)	I2···H04C	3.211(7)	3.125(1)
F03···H13	2.549(18)	2.821(16)	I2···C04	4.004(14)	4.019(15)
F03···C13	3.416(19)	3.687(18)	\angle I2···H04C-C04	139.2(9)	155.6(10)
\angle F03···H13-C13	152.0(7)	155.4(8)	Acetone-CF₃SO₃		
F03···H27	2.643(23)	2.819(22)	F02···H04B	2.598(21)	2.686(20)
F03···C27	3.472(19)	3.570(24)	F02···C04	3.370(10)	3.524(27)
\angle F03···H27-C27	152.0(7)	138.5(7)	\angle F02···H04B-C04	135.7(10)	146.1(11)

Table S13 Intermolecular interactions within **6** at 123 K.

A-B…X	B…X/Å	A…X/Å	∠ A-B…X/°
1D chain along b axis			
π-π	3.269		
I2…π	3.567		
π-π	3.265		
O2…H7-C7	2.592(7)	3.466(1)	153.3(5)
along c axis			
P4AE			
π-π	3.682		
C13-H13…π	2.672		
Along a axis			
I2…π	3.494		
CF₃SO₃			
O3…H3-C3	2.609(7)	3.379(1)	138.4(5)
O3…H30-C30	2.703(6)	3.368(11)	127.6(5)
O3…I1	3.120(7)		
O4…H2-C2	2.429(7)	3.333(12)	158.7(5)
O4…H15-C15	2.582(8)	3.460(13)	154.0(6)
O4…H23-C23	2.666(6)	2.839(10)	90.5(5)
O5…H14-C14	2.568(8)	3.195(14)	123.8(6)
F3…H26-C26	2.464(6)	3.187(12)	132.8(6)
F2…π(C _g C10-C11)	3.014		
MeCN			
N5…H18-C18	2.624(11)	3.389(14)	137.7(5)
N5…H31-C31	2.520(11)	3.412(15)	156.5(6)
CF ₃ SO ₃ -MeCN			
O5…H34B-C34	2.770(7)	3.334(13)	117.2(6)

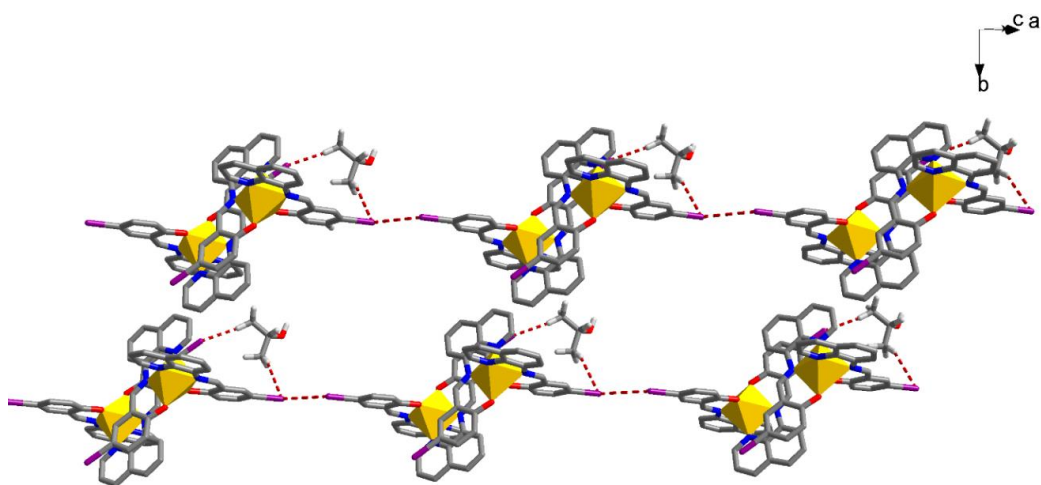


Figure S8 The I···I interaction in **4**. Similar interactions occur in the other solvates.

Table S14 P4AE interactions in $[\text{Fe}(\text{qsal}-\text{I})_2]\text{OTf}\cdot\text{sol}$.

Solvent	T/K		
	163 K	230 K	293 K
MeOH			
π-π	3.371	3.366	3.468
C33-H33···π	2.467	2.513	2.569
EtOH	100 K	170 K	213 K
π-π	3.062	3.444	3.467
C29-H29···π	2.607	2.540	2.592
n-PrOH	100K	270 K	
π-π	3.091	3.255	
C13-H13···π	2.578	2.598	
<i>i</i> -PrOH	163 K	293 K	
C26-H26···π	2.762	2.783	
Acetone	137 K	293 K	
π···π	3.551	3.606	
C44-H44···π	3.179	3.303	
MeCN	123 K		
π-π	3.682		
C13-H13···π	2.672		

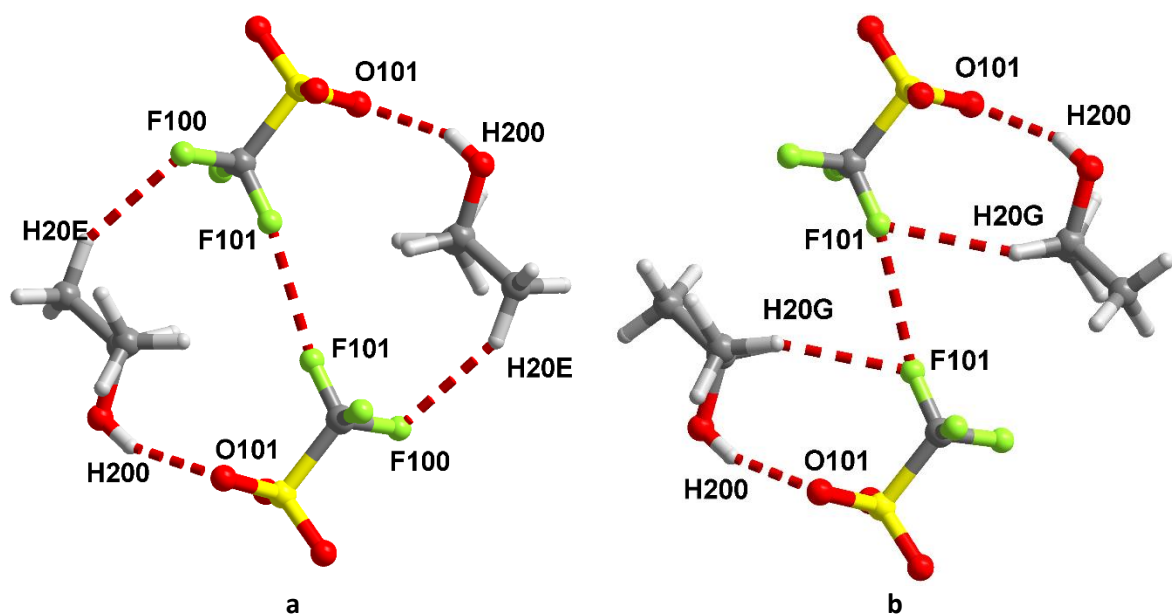


Figure S9 The supramolecular solvent-anion circle in **4** at a) 163 and b) 293 K.

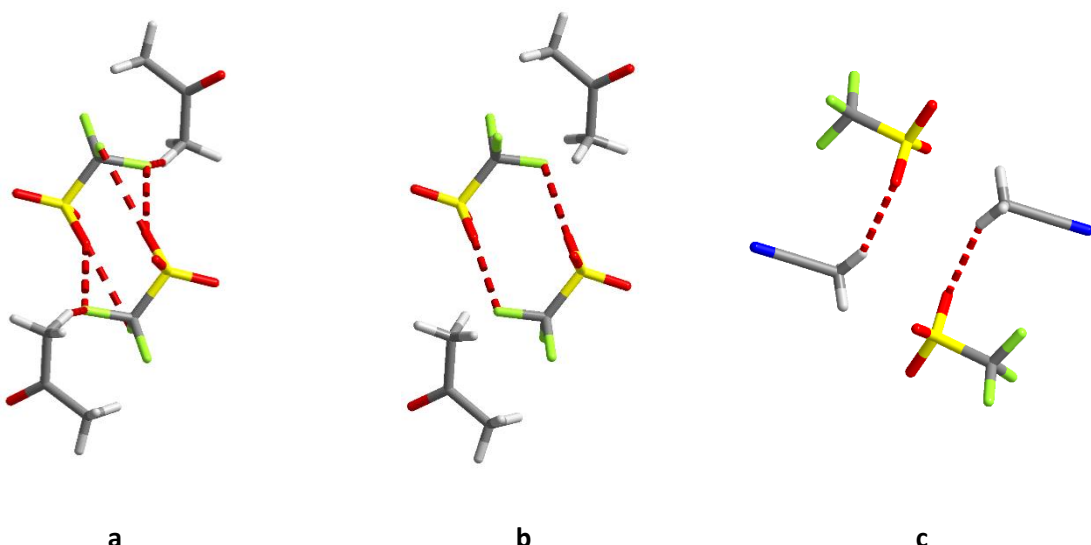


Figure S10 Supramolecular interactions of the acetone molecules and triflate anions in **5** at a) 137 K and b) 293 K and c) in **6**.

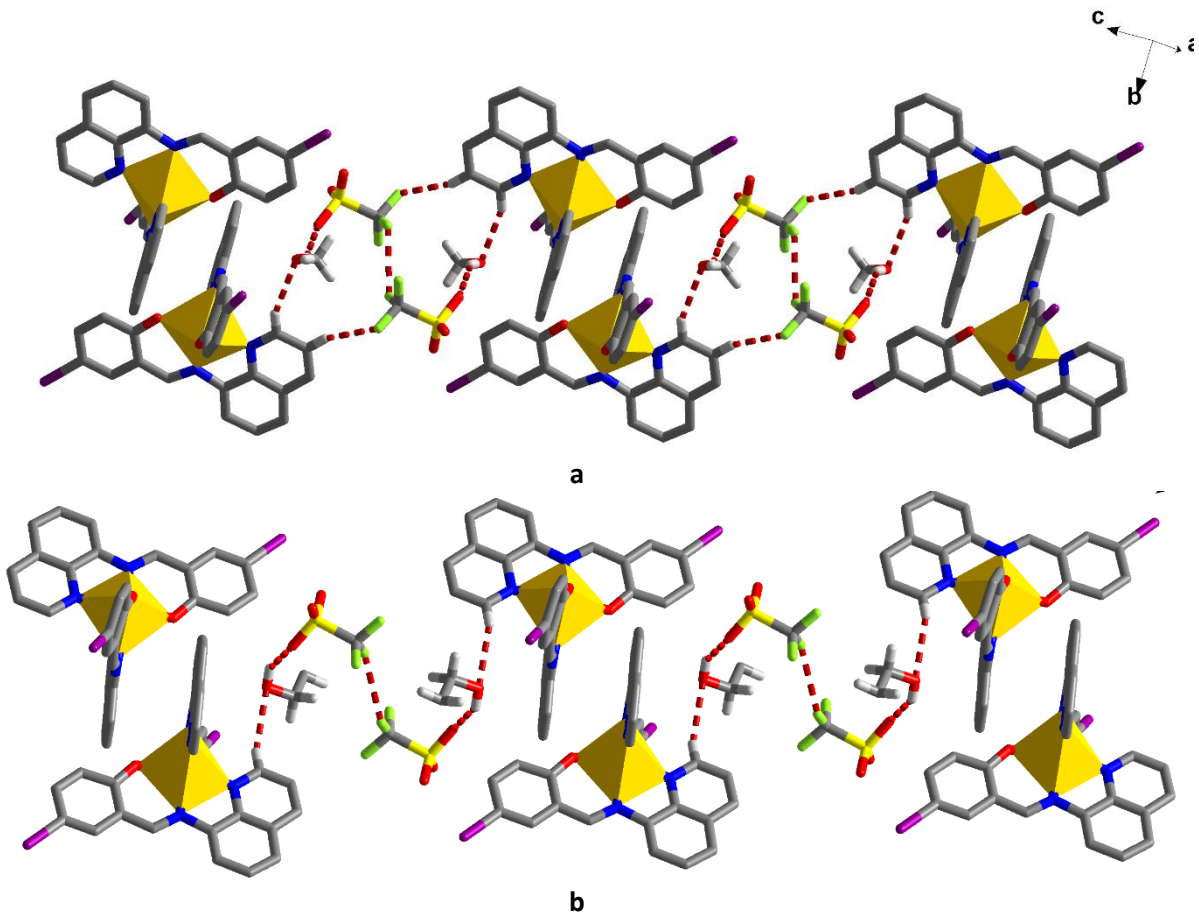
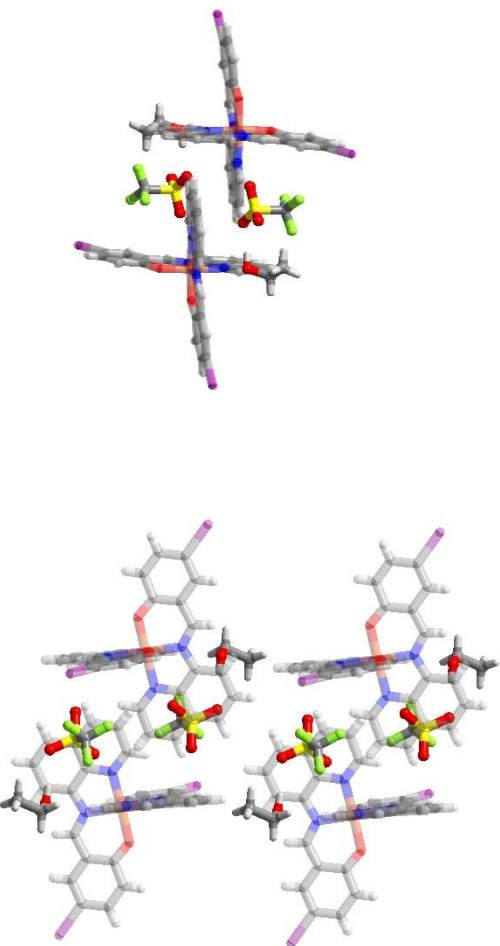


Figure S11 C-H...F/O interactions related to triflate and MeOH/EtOH solvates bridging the Fe moieties in a) **1** and b) **2**.

Table S15 Supramolecular interactions involving the triflate anion and solvent molecules.

Solvent	T/K		
	163 K	230 K	293 K
MeOH			
F2···F3	3.005(15)	2.991(13)	2.867(17)
O1O1···H2O0	2.087(9)	2.014(6)	2.089(10)
EtOH	100 K	170 K	213 K
F2···F2	2.719(8)	2.865(5)	2.904(13)
O5···H6 (O4-LS)	2.109(6)	2.053(4)	2.103(8)
n-PrOH	100K	270 K	
F2···F2	2.713(4)	2.809(6)	
H6···O5	2.162(3)	2.200(5)	
H34A···F1	2.540(3)	2.724(4)	
H36C···O5	2.653(4)	2.922(6)	
i-PrOH	163 K	293 K	
F1O1···F1O1	2.760(11)	2.843(10)	
O1O1···H2O0	2.020(8)	1.903(8)	
F1O1···H2O G	2.826(12)	2.641(12)	
F100···H2O E	2.571(18)	3.440(18)	

100 K, phase 2b



170 K, phase 2a

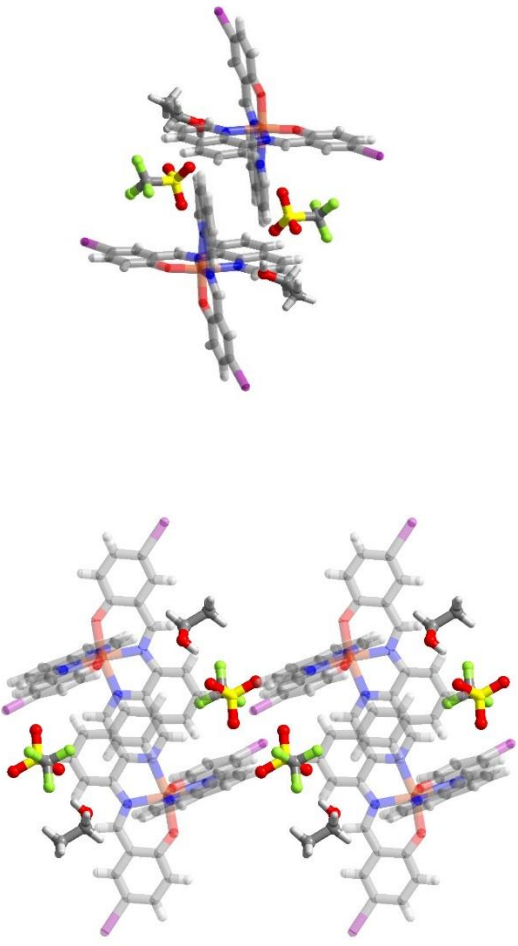


Figure S12 View of the repositioning of the triflate anion following spin crossover in $[\text{Fe}(\text{qsal}-\text{I})_2]\text{OTf}\cdot\text{EtOH}$ 2.

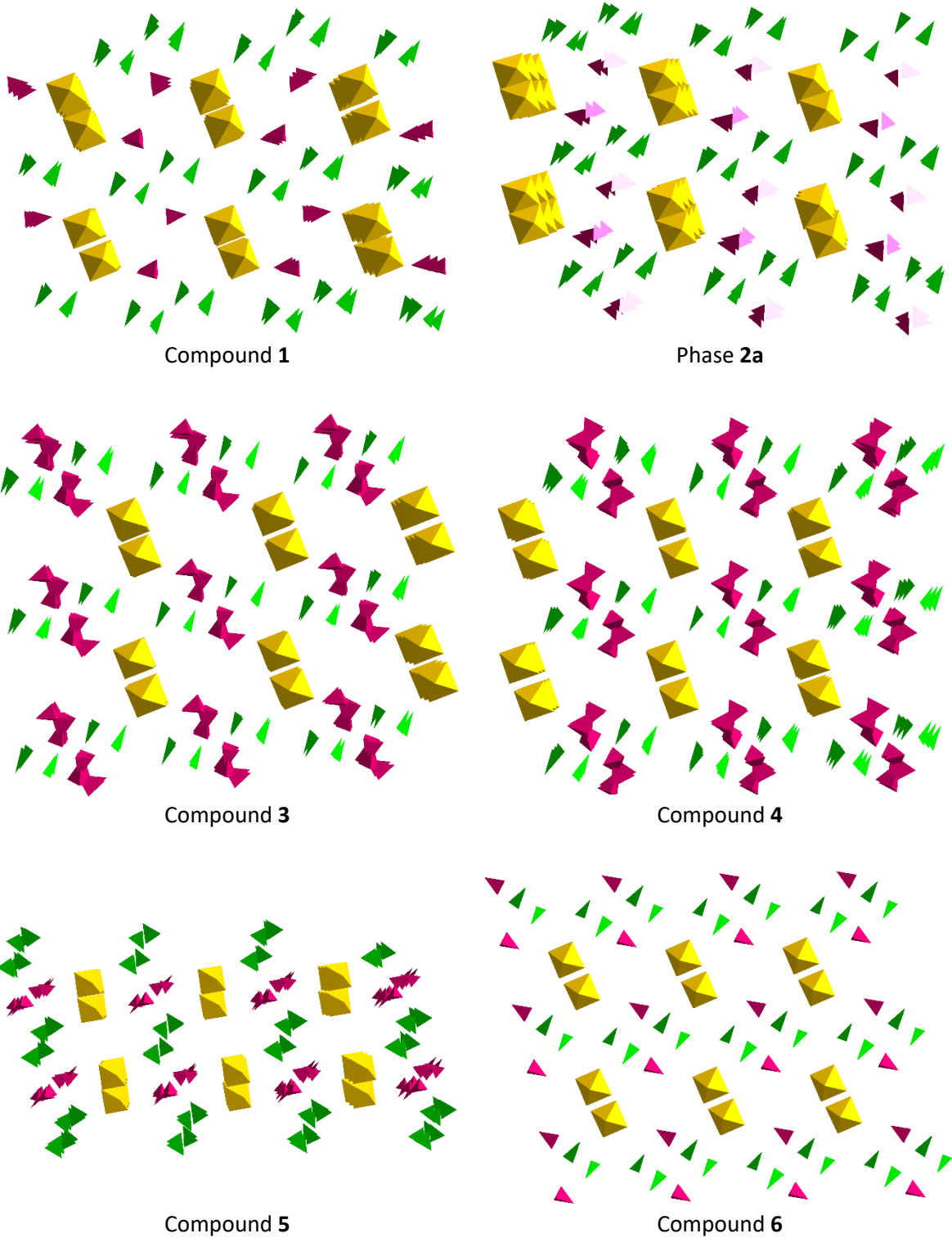


Figure S13 Simplified packing diagram of **1-6** with the $[\text{Fe}(\text{qsal-}\text{I})_2]^+$ cations shown in yellow, the triflate anions in green and the solvent molecules in burgundy.